Photodissociation of Acetone in Air: Dependence on Pressure and Wavelength. Behavior of the Excited Singlet State

Martin Emrich[†] and Peter Warneck*

Max-Planck-Institut für Chemie, 55020 Mainz, Germany

Received: May 22, 2000; In Final Form: August 4, 2000

Quantum yields of acetyl radicals resulting from the photodissociation of 0.1−1% acetone in air were studied in the wavelength range 280−330 nm and at total pressures ranging from 130 to 1000 hPa. Through the addition of small amounts of NO_2 to the gas mixtures, acetyl peroxy radicals were scavenged to form peroxyacetyl nitrate (PAN). The PAN quantum yields obeyed a Stern−Volmer type pressure dependence at all wavelengths studied. The experimental data were combined with results from the literature to derive the rate of photodissociation from the excited singlet state of acetone and the competing intersystem crossing rate populating the triplet state, both relative to that of pressure quenching, as a function of energy above the dissociation threshold. The rate of photodissociation was found to increase with excitation energy, whereas that of intersystem crossing shows a maximum at intermediate energies. Previously reported quantum yields for CO formation were analyzed to allow comparison with acetyl radical production.

Introduction

The photochemistry of acetone in the gas phase has been extensively studied and several reviews are available.[1−6] The main primary photodecomposition process following excitation within the first absorption band in the near-ultraviolet spectral region is dissociation toward methyl and acetyl radicals

$$CH_3COCH_3^* \rightarrow CH_3 + CH_3CO \qquad (1)$$

The $^1(n-\pi^*)$ transition responsible for the absorption band populates initially various levels of the first excited singlet state S_1, but internal energy conversion channels much of the available energy into other accessible states, mainly to the lower-lying triplet state T_1, possibly also to high-lying vibrational levels of the S_0 ground state. Dissociation may occur from all three states provided there is sufficient energy in vibrational excitation to overcome a dissociation barrier. The existence of such a barrier was suggested because of the influence of temperature on the product yield,[5,7] especially that of CO. The triplet state is distinguished from the singlet by a longer-lasting emission to the ground state (phosphorescence) as opposed to prompt emission from S_1 (fluorescence). The fluorescence/phosphorescence emission kinetics has been studied at low pressures (about 0.1 Pa) by means of nanosecond pulse laser excitation.[8−11] The results clearly demonstrated the occurrence of four basic processes with increasing time constants: fast intersystem crossing ($\leq$10 ns), fluorescence from S_1 ($\sim$3 μs), phosphorescence from vibrationally hot triplet levels ($\sim$30 μs), and emission from the thermalized triplet state (200 μs). Previous work has established important reactive properties of acetone excited to the triplet state when compared to the singlet. Triplet acetone is rapidly quenched by oxygen,[11,12] causes the isomerization of 1,2-disubstituted alkenes,[13] and undergoes efficient energy transfer to 2,3-butadione (biacetyl) and various aldehydes.[14] The last two phenomena have been used to estimate an S_1-T_1 crossing yield near unity at 313 nm, which was the favored wavelength used in most photochemical studies. The phosphorescence intensity declines toward shorter wavelengths,[15,16] indicating either that the efficiency of intersystem crossing declines as well or that it can no longer compete with acetone photodissociation.

The present study evolved from our interest in the behavior of acetone in the atmosphere and its photodecomposition in the presence of sunlight. In this context, the dependence of quantum yields on wavelength and pressure is important, and the present paper deals with this aspect. Gierczak et al.[17] recently presented quantum yields for acetone loss and CO_2 production in air as a carrier gas. Meyrahn et al.[18] have shown how one can determine the quantum yield of acetyl radicals in air from the yield of peroxyacetyl nitrate (PAN) formed when nitrogen dioxide is added as a radical scavenger. The reactions involved are

$$CH_3CO + O_2 \rightarrow CH_3CO_3 \qquad (2)$$

$$CH_3CO_3 + NO_2 \rightarrow CH_3C(O)O_2NO_2\ (PAN) \qquad (3)$$

Although PAN is thermally unstable, its decomposition in the gas phase is still so slow at 25 °C that it may be ignored within the time scale of such experiments. Meyrahn et al.[18] have measured PAN quantum yields of acetone in air in the wavelength range 250−330 nm but only at atmospheric pressure. In the pressure range explored here, 130−1000 hPa, triplet acetone is expected to be completely quenched by oxygen. Accordingly, this state should not contribute significantly to the formation of acetyl radicals. The data may be extrapolated toward lower pressures, however, and thereby the results can also provide information on the extent of triplet acetone formation as a function of wavelength. We will show that a synthesis of our results with earlier data provides a unified picture of acetone photolysis under these conditions.

Experimental Section

Parts of the experimental setup have been described previously.[18,19] Briefly, light from a 150 W xenon arc lamp was wavelength-selected with an *f*/2 monochromator adjusted to a

* To whom correspondence should be addressed. Fax number: +49−6131−305487. E-mail: biogeo@mpch-mainz.mpg.de.

[†] Present address: Saarberg-Interplan, 66115 Saarbrücken, Germany.

10.1021/jp001873i CCC: $19.00
Published on Web 09/29/2000

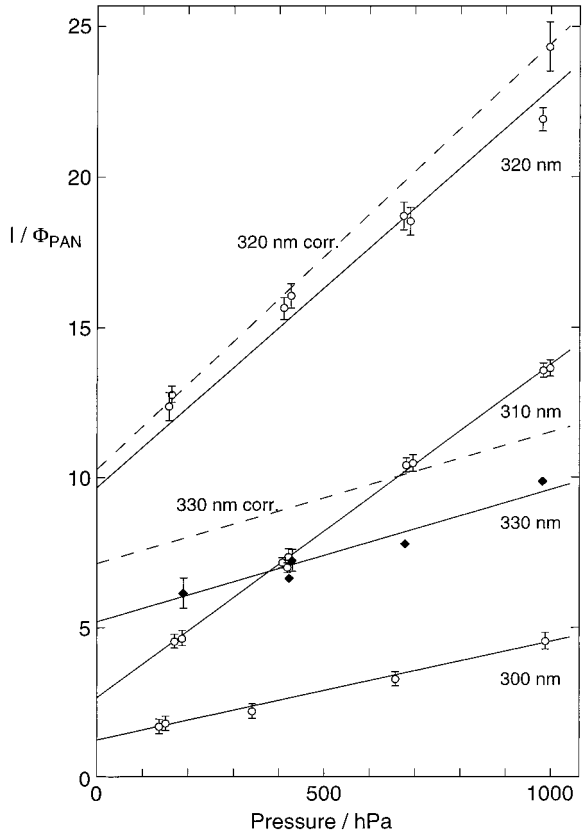

Figure 1. Stern−Volmer plots of reciprocal PAN quantum yields versus pressure of the acetone/air mixture. Wavelengths are indicated on the right. The dashed lines were obtained after corrections for NO_2 photodissociation at the two longest wavelengths used (see text).

spectral resolution of 4 nm at half-width. The light emerging from the monochromator exit slit was recollimated to pass end-on through a cylindrical quartz cell (10 cm long, 1.8 cm i.d). The transmitted radiation flux was determined and monitored with a calibrated thermopile. A gas handling manifold served to fill the photolysis cell to the desired pressure with synthetic air containing mole fractions of about 13 μmol mol^{-1} NO_2 and 0.1−1% acetone. Pressures were measured with calibrated capacitance manometers.

Gas chromatography was used to analyze the contents of the photolysis cell immediately following irradiation. The instrument combined a packed glass column with a home-built NO−O_3 chemiluminescence detector.[20] The column, 50 cm long, 3.7 mm i.d., was packed with 10% Carbowax 600 on Chromosorb (80−100 mesh). The gases eluting from the column first passed through a molybdenum catalytic converter heated to 350 °C to decompose PAN and other organic nitrates before entering the detector. Samples were injected by expanding a portion of the irradiated gas mixture from the photolysis cell into an evacuated sampling loop, which was then switched into the nitrogen carrier gas flow by the inlet valve. As a consistency check, three samples usually were analyzed, and the results were averaged. The system was calibrated with a mixture of 1.7 μmol mol^{-1} NO in nitrogen. The equivalence of using either NO or PAN to calibrate the system has been demonstrated previously.[21] Peak areas were determined with an integrating recorder. Schurath et al.[22] have shown that PAN suffers losses on gas chromatographic columns, the losses increasing with the retention time. For retention times of 2.8 min, as observed in this study, the correction amounts to 20%. In the previous experiments, the effect was smaller because a shorter column was used. The possible error associated with the correction contributed 90% to the total systematic error, which amounted to 8.5%, whereas the statistical error was about 4%.

Losses also occurred in the photolysis cell due to the wall-catalyzed thermal decomposition of PAN. Conditioning the walls by repeated exposure to PAN/air mixtures greatly reduced such losses. The measured half-lifetime of PAN in the conditioned cell was 9.1 h at 25 °C and 1000 hPa, shorter than in larger vessels[21] but still sufficiently long to make losses insignificant except when extensive photolysis times were employed.

Results

PAN concentrations in irradiated mixtures rose linearly with time up to quite high NO_2/PAN conversion ratios. In the present work, the conversion was kept below 30%, but checks for linearity were made under all experimental conditions.

PAN quantum yields were calculated from the total amount of product and the radiation dose delivered into the photolysis cell. Absorption cross sections for acetone at the wavelengths used were taken from Gierczak et al.[17] In the wavelength range covered, their data agree well with our earlier values.[18] As previously, the radiation dose was calculated from the photon flux through the cell ($\sim 10^{15}$ photon cm^{-2} s^{-1}), the fraction of radiation absorbed by acetone (0.2%−4%), and the applied irradiation time (300−3600 s). Wavelengths were set at 10 nm intervals in the spectral region 280−330 nm. Table 1 shows experimental conditions and the resulting quantum yields grouped according to wavelength, pressure, and irradiation time. The data were then used to generate Stern−Volmer plots of reciprocal quantum yields versus pressure. Straight lines were obtained at all wavelengths. Figure 1 shows a number of such plots for several series of measurements. The data were subjected to a least-squares regression analysis, and Table 2 summarizes the results in terms of slopes and intercepts with the ordinate. At wavelengths equal to or smaller than 300 nm, the intercepts are in the vicinity of unity, whereas at longer wavelengths the intercepts are consistently greater. The slopes generally increase with increasing wavelength, but the trend is reversed at 330 nm. Although fewer data are available at this wavelength, they still obey a linear Stern−Volmer relationship.

At most wavelengths, the chosen mixing ratio of acetone was high enough relative to that of NO_2 to make photodissociation of NO_2 comparatively insignificant. Under the optically thin conditions used in the experiments, the influence of NO_2 photolysis on PAN quantum yields is determined by the ratio $\sigma_{NO_2}[NO_2]/\sigma_{acet}[acetone]$, where σ_{NO_2} and σ_{acet} denote the absorption cross sections of NO_2 and acetone, respectively. At all wavelengths of $\leq$ 320 nm, it was possible to keep the ratio at 0.06 or less, but at 330 nm it became larger, almost 0.5. As a consequence, the data taken at 330 nm are impaired by an undesirable high degree of NO_2 photodissociation. The NO thus generated reacts partly with CH_3O_2, which is a product from acetone photolysis, and subsequent reaction leads to the formation of OH. The OH radicals, in turn, react with acetone to produce additional CH_3CO_3 whereby the yield of PAN is raised. Accordingly, the true PAN quantum yields must be smaller than the observed values. The impact of this effect was explored by means of computer simulations based on the reaction scheme shown in Table 3. The leading reactions are indicated by asterisks. Reactions involving the breakdown of acetone via the acetonyl peroxy radical were taken from Jenkin et al.[23] Wollenhaupt and Crowley[24] recently demonstrated that the reaction of OH with acetone proceeds along two channels, one leading to acetonyl and the other to methyl and acetic acid as products. This feature was incorporated in the mechanism. Although most of the other reactions, especially the self- and

TABLE 1: PAN Quantum Yields as a Function of Pressure at Different Wavelengths (NO_2/Air Mole Fraction = 13.93 ± 0.07 μmol mol^{-1})

p (hPa)	t (s)	x(PAN) (μmol/mol)	Φ	n^a	p (hPa)	t (s)	x(PAN) (μmol/mol)	Φ	n^a
λ = 280 nm, x(acetone) = 1.002 mmol/mol, $I_0 \approx 3.78 \times 10^{14}$ photon/s									
1007 ± 4	304	1.48 ± 0.03	0.77 ± 0.02	3	349 ± 1	303	1.84 ± 0.02	0.99 ± 0.01	3
995 ± 5	304	1.48 ± 0.02	0.79 ± 0.01	4	345 ± 1	453	2.79 ± 0.04	1.01 ± 0.01	3
981 ± 3	153	0.77 ± 0.01	0.80 ± 0.01	3	341 ± 1	153	0.94 ± 0.01	1.00 ± 0.01	3
966 ± 3	453	2.36 ± 0.02	0.84 ± 0.01	3	153 ± 1	303	1.74 ± 0.02	0.94 ± 0.01	4
745 ± 3	303	1.61 ± 0.01	0.86 ± 0.01	4	151	453	2.68 ± 0.04	0.97 ± 0.02	3
732 ± 3	153	0.83 ± 0.02	0.86 ± 0.03	3	149	603	3.67 ± 0.07	1.00 ± 0.02	3
724 ± 2	453	2.51 ± 0.03	0.89 ± 0.01	3					
λ = 290 nm, x(acetone) = 1.002 mmol/mol, $I_0 \approx 4.97 \times 10^{14}$ photon/s									
989 ± 3	303	1.24 ± 0.01	0.60 ± 0.01	3	345 ± 3	303	1.88 ± 0.03	0.93 ± 0.02	4
976 ± 6	453	1.88 ± 0.01	0.61 ± 0.01	4	339 ± 3	603	3.74 ± 0.02	0.94 ± 0.01	5
959 ± 4	603	2.47 ± 0.02	0.61 ± 0.01	3	332 ± 2	453	2.83 ± 0.03	0.96 ± 0.01	4
677 ± 4	303	1.50 ± 0.01	0.73 ± 0.01	4	153	303	2.07 ± 0.01	1.04 ± 0.01	3
664 ± 4	603	3.02 ± 0.04	0.74 ± 0.01	5	152 ± 1	453	3.09 ± 0.07	1.04 ± 0.02	4
652 ± 5	453	2.31 ± 0.02	0.76 ± 0.01	5	149	603	4.06 ± 0.02	1.03 ± 0.01	4
λ = 300 nm, x(acetone) = 0.998 mmol/mol, $I_0 \approx 6.61 \times 10^{14}$ photon/s									
996	454	0.545	0.205	1	344 ± 3	904	2.41 ± 0.03	0.46 ± 0.01	5
994	604	0.745	0.212	1	148	304	0.99 ± 0.02	0.56 ± 0.02	2
992	754	0.944	0.213	1	147	454	1.40 ± 0.02	0.53 ± 0.01	2
989	904	1.153	0.217	1	145	604	2.03 ± 0.09	0.57 ± 0.03	3
985	1054	1.375	0.221	1	144	904	2.990	0.564	1
991 ± 6	average of above data		0.214 ± 0.005	6	144	754	2.550	0.579	1
661 ± 4	904	1.60 ± 0.04	0.31 ± 0.01	5	143	1054	3.468	0.562	1
λ = 310 nm, x(acetone) = 3.019 mmol/mol, $I_0 \approx 6.26 \times 10^{14}$ photon/s									
742	303	0.197	0.076	1	692 ± 4	603	0.51 ± 0.01	0.096 ± 0.003	5
997 ± 4	603	0.38 ± 0.01	0.073 ± 0.001	3	683 ± 3	1203	1.89 ± 0.01	0.097 ± 0.001	3
981 ± 4	1204	1.42 ± 0.01	0.073 ± 0.001	3	421 ± 3	603	0.68 ± 0.01	0.134 ± 0.004	4
697 ± 3	303	0.25 ± 0.01	0.095 ± 0.001	3					
λ = 310 nm, x(acetone) = 10.757 mmol/mol, $I_0 \approx 3.34 \times 10^{14}$ photon/s									
416	603	1.36 ± 0.01	0.14 ± 0.01	2	160 ± 1	603	2.05 ± 0.04	0.22 ± 0.01	4
418 ± 3	1203	2.75 ± 0.02	0.14 ± 0.01	3	157 ± 1	1203	4.10 ± 0.04	0.21 ± 0.01	3
λ = 320 nm, x(acetone) = 10.867 mmol/mol, $I_0 \approx 6.57 \times 10^{14}$ photon/s									
997 ± 5	603	0.26 ± 0.01	0.041 ± 0.002	5	428 ± 3	904	0.59 ± 0.01	0.062 ± 0.001	4
985 ± 4	1203	0.59 ± 0.01	0.046 ± 0.001	2	421 ± 3	1804	1.22 ± 0.02	0.064 ± 0.002	3
693 ± 4	603	0.35 ± 0.01	0.054 ± 0.001	4	161 ± 1	1204	1.02 ± 0.03	0.080 ± 0.003	4
685 ± 3	1203	0.68 ± 0.02	0.054 ± 0.001	4	160	2403	1.97 ± 0.01	0.078 ± 0.001	3
λ = 330 nm, x(acetone) = 10.867 mmol/mol, $I_0 \approx 7.02 \times 10^{14}$ photon/s									
976	1204	0.235	0.101	1	417 ± 1	3603	0.93 ± 0.02	0.134 ± 0.01	2
677	1204	0.294	0.127	1	160 ± 1	3603	1.08 ± 0.03	0.163 ± 0.01	2
419	1803	0.505	0.148	1					

[a] Number of runs.

TABLE 2: Linear Regression Parameters of Stern−Volmer Plots of Reciprocal Quantum Yields and Triplet Quantum Yields at Various Wavelengths

λ/nm	intercept	10^3 slope/hPa	r^a	Φ_S	Φ_T
280	0.96 ± 0.03	0.28 ± 0.05	0.907	1.05 ± 0.03	~0
290	0.93 ± 0.03	0.71 ± 0.05	0.981	1.07 ± 0.04	~0
300	1.19 ± 0.06	3.37 ± 0.11	0.992	0.84 ± 0.04	0.16 ± 0.04
310	2.65 ± 0.26	11.38 ± 0.39	0.997	0.38 ± 0.04	0.62 ± 0.04
320	9.75 ± 0.75	13.36 ± 1.10	0.980	0.10 ± 0.01	0.90 ± 0.01
320[b]	10.23 ± 0.79	14.38 ± 1.19	0.980	0.10 ± 0.01	0.90 ± 0.01
330	5.19 ± 0.40	4.36 ± 0.64	0.980	0.19 ± 0.01	0.83 ± 0.01
330[b]	7.10 ± 0.55	4.45 ± 0.65	0.980	0.10 ± 0.01	0.86 ± 0.01

[a] Correlation coefficient. [b] Individual data corrected for the influence of NO_2 photolysis.

cross-combination reactions of peroxy radicals, were of marginal significance, they were retained for consistency in the total mechanism. The Facsimile[26] computer code was used for the calculations. Rate constants for the photolysis of NO_2 and acetone represent experimental conditions. The quantum yield of acetone photolysis was varied until the quantum yield calculated from the yield of PAN matched that observed in the experiments. The results of the calculations are shown in Figure 1 by the dashed lines. At 330 nm wavelength, the correction required was substantial, at 320 nm it was marginal (less than 10%), and at 310 nm and shorter wavelengths it was negligible. In fact, as Table 1 shows, in the runs at 310 nm, a change in acetone mixing ratio by a factor of 3 did not have any noticeable effect on the behavior of the experimentally observed quantum yield. Table 2 includes Stern−Volmer parameters for the corrected quantum yields at 320 and 330 nm wavelength. In the latter case, the intercept with the ordinate is raised considerably so that it approaches that at 320 nm, but the slope changes little, so it still differs substantially from that at 320 nm.

In the wavelength region 300−320 nm, the PAN quantum yields at pressures close to 1000 hPa are greater by a factor of about 1.4 than those found by Meyrahn et al.[18] at the same pressure. The reason for the difference is difficult to assess. It may be associated with the correction factors applied to account for PAN losses, although it is much greater than the sum of experimental errors (<10%). At 330 nm, the present quantum yield for 1000 hPa pressure is 3 times higher than that reported by Meyrahn et al.[18] The acetone/NO_2 ratio in their study was about twice that used here, so the impact of NO_2 photodissociation should have been correspondingly smaller.

Discussion

The present data provide quantum yields in air for acetyl radicals from the photodissociation of acetone. Reaction with oxygen converts acetyl to acetyl peroxy radicals, and these

TABLE 3: Reaction Mechanism Used for the Simulation of Acetone Photolysis in the Presence of NO_2 at 330 nm Wavelength[a]

	reaction	k^b
1*	$CH_3COCH_3 \rightarrow CH_3 + CH_3CO$	1.73 (−7) ϕ
2*	$CH_3 + O_2 \rightarrow CH_3O_2$	rapid
3*	$CH_3CO + O_2 \rightarrow CH_3CO_3$	rapid
4*	$NO_2 \rightarrow NO + O$	1.10 (−4)
5	$O + O_2 + M \rightarrow O_3 + M$	5.8 (−34)
6	$O + NO_2 \rightarrow NO$	9.7 (−12)
7	$O + NO_2 + M \rightarrow NO_3 + M$	8.0 (−32)
8	$NO + O_3 \rightarrow NO_2 + O_2$	1.8 (−14)
9	$NO_2 + O_3 \rightarrow NO_3$	3.2 (−17)
10	$NO + NO_3 \rightarrow NO_2 + NO_2$	2.7 (−11)
11	$NO_2 + NO_3 \rightarrow N_2O_5$	1.2 (−12)
12	$N_2O_5 \rightarrow NO_2 + NO_3$	6.1 (−2)
13	$NO + CH_3CO_3 \rightarrow NO_2 + CH_3 + CO_2$	1.4 (−11)
14*	$NO_2 + CH_3CO_3 \rightarrow PAN$	8.0 (−12)
15	$PAN \rightarrow NO_2 + CH_3CO_3$	5.5 (−4)
16*	$NO + CH_3O_2 \rightarrow CH_3O + NO_2$	7.6 (−12)
17	$NO_2 + CH_3O_2 \rightarrow CH_3O_2NO_2$	5.2 (−12)
18	$CH_3O_2NO_2 \rightarrow CH_3O_2 + NO_2$	2.5
19*	$NO + CH_3COCH_2O_2 \rightarrow CH_3COCH_2O + NO_2$	8.0 (−12)
20*	$HO_2 + NO \rightarrow OH + NO_2$	8.3 (−12)
21	$OH + NO_2 \rightarrow HNO_3$	1.2 (−11)[c]
22a*	$OH + CH_3COCH_3 \rightarrow CH_3COCH_2 + H_2O$	1.15 (−13)
22b*	$OH + CH_3COCH_3 \rightarrow CH_3COOH + CH_3O_2$	1.15 (−13)
23*	$CH_3COCH_2 + O_2 = CH_3COCH_2O_2$	rapid
24a	$2\ CH_3COCH_2O_2 \rightarrow CH_3COCHO + CH_3COCH_2OH + O_2$	4.0 (−12)
24b	$2\ CH_3COCH_2O_2 \rightarrow 2\ CH_3COCH_2O + O_2$	4.0 (−12)
25	$CH_3COCH_2O + O_2 \rightarrow CH_3COCHO + HO_2$	9.5 (−15)
26*	$CH_3COCH_2O \rightarrow CH_3CO + HCHO$	1.0 (6)
27	$CH_3CO_3 + CH_3CO_3 \rightarrow CH_3 + CH_3 + CO_2 + CO_2 + O_2$	1.6 (−11)
28a	$CH_3O_2 + CH_3O_2 \rightarrow HCHO + CH_3OH$	2.4 (−13)
28b	$CH_3O_2 + CH_3O_2 \rightarrow CH_3O + CH_3O$	1.3 (−13)
29*	$CH_3O + O_2 \rightarrow HCHO + HO_2$	1.9 (−15)
30a	$CH_3COCH_2O_2 + CH_3CO_3 \rightarrow CH_3COCHO + CH_3COOH + O_2$	2.7 (−12)
30b	$CH_3COCH_2O_2 + CH_3CO_3 \rightarrow CH_3COCH_3O + CH_3 + CO_2 + O_2$	2.3 (−12)
31a	$CH_3COCH_2O_2 + CH_3O_2 \rightarrow CH_3COCH_2OH + HCHO + O_2$	6.0 (−13)
31b	$CH_3COCH_2O_2 + CH_3O_2 \rightarrow CH_3COCHO + CH_3OH + O_2$	2.0 (−12)
31c	$CH_3COCH_2O_2 + CH_3O2 \rightarrow CH_3COCH_2O + CH_3O + O_2$	1.2 (−12)
32a	$CH_3O_2 + CH_3CO_3 \rightarrow CH_3 + CH_3O + CO_2 + O_2$	5.5 (−12)
32b	$CH_3O_2 + CH_3CO_3 \rightarrow CH_3COOH + HCHO + O_2$	5.5 (−12)
33	$HO_2 + HO_2 \rightarrow H_2O_2$	2.8 (−12)
34	$HO_2 + CH_3COCH_2O_2 \rightarrow CH_3COCH_2OOH$	9.0 (−12)
35	$HO_2 + CH_3O_2 \rightarrow CH_3OOH$	5.8 (−12)
36	$HO_2 + CH_3CO_3 \rightarrow CH_3C(O)OOH;$	8.5 (−12)
37	$HO_2 + CH_3CO_3 \rightarrow CH_3COOH + O_3$	4.5 (−12)

[a] The leading reactions involved in PAN formation are indicated by asterisks. Rate constants were taken from Jenkin et al.[23] and Atkinson et al.[25] [b] In units of cm^3, molecule, s, powers of 10 in parentheses. [c] Rate coefficient at ~1000 hPa pressure.

radicals are stabilized by the addition of NO_2 to form PAN. In the Introduction, it was pointed out that triplet acetone is rapidly quenched by oxygen at rather low pressures, so the triplet state cannot be held responsible for the formation of acetyl radicals. Thus, the observed quantum yields and the pressure dependence must involve the single state, and we interpret the results in terms of the following simple mechanism:

$$S_0 + h\nu \rightarrow S_1 \qquad \text{(a)}$$

$$S_1 \rightarrow T_1^* \qquad k_{ISC} \qquad \text{(b)}$$

$$T_1^* + O_2 \rightarrow S_0 + O_2 \qquad \text{rapid} \qquad \text{(c)}$$

$$S_1 \rightarrow CH_3 + CH_3CO \qquad k_D \qquad \text{(d)}$$

$$S_1 + M \rightarrow T_1^* + M \qquad {}^1k_M \qquad \text{(e)}$$

$$S_1 + M \rightarrow S_0 + M \qquad {}^2k_M \qquad \text{(f)}$$

Similar mechanisms have been discussed in earlier studies.[6,7,12,13,16] Fluorescence from the excited singlet state has a low probability and is neglected here. However, internal energy conversion induced by collisions, process e, is included because Gandini and Hackett[16] had found that intersystem crossing is accelerated by increasing the pressure of CO_2, which they used as an inert quenching gas. Because of rapid quenching of T_1^* by oxygen, we cannot differentiate between processes e and f, and they may be combined by setting $k_M = {}^1k_M + {}^2k_M$. Our experimental data can be combined with those of others to derive information on the behavior of the S_1 state as a function of excitation energy, and this aspect will set the main theme of the following discussion.

With the assumption that the acetyl peroxy radicals resulting from process d are completely converted to PAN via reactions 1−3, the above mechanism leads to the dissociation quantum yield

$$\Phi_{diss} = \frac{k_D}{k_D + k_{ISC}} \Big/ \left(1 + \frac{k_M[M]}{k_D + k_{ISC}}\right) \qquad (4)$$

and the inverse

$$1/\Phi_{diss} = 1/\Phi_S + (k_M/k_D)[M] \qquad (5)$$

where $[M] = 2.46 \times 10^{16}\ p$ [hPa] is the total gas concentration (at $T \approx 296$ K), essentially equivalent to that of the air carrier gas, and $\Phi_S = k_D/(k_{ISC} + k_D)$ is the zero pressure quantum yield

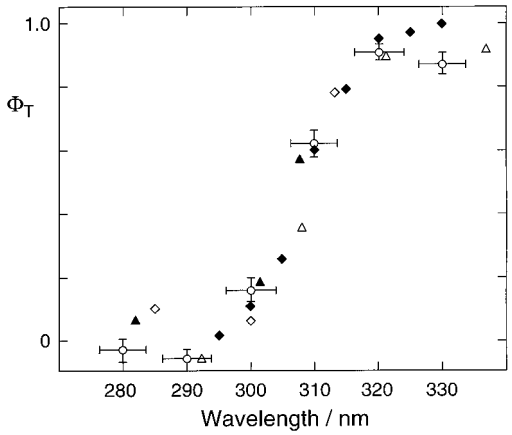

Figure 2. Acetone triplet quantum yield as a function of wavelength: open points show present data (vertical bars indicate 2s statistical error, horizontal bars show full wavelength range); solid and open triangles were derived from data reported by Gierczak et al.[17] for acetone loss and CO_2 formation, respectively; open diamonds were taken from Horowitz;[6] solid diamonds are intersystem crossing quantum yields that were read off a graph presented by Gandini and Hackett.[16]

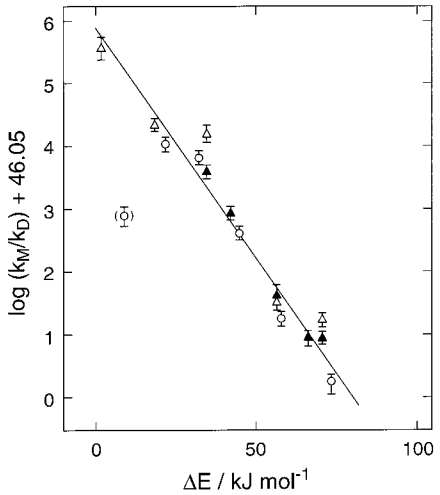

Figure 3. Natural logarithm of $10^{20}k_M/k_D$ plotted versus energy above the dissociation threshold. The data were derived from the slopes of Stern−Volmer plots (present data and data from Gierczak et al.,[17] symbols as in Figure 2). The linear regression line shown, which is represented by $\log_e(10^{20}k_M/k_D) = (5.92 \pm 0.23) - (0.073 \pm 0.005)\Delta E$, omits our point at $\lambda = 330$ nm, shown in parentheses.

([M] = 0). Similarly, the triplet quantum yield at zero pressure is $\Phi_T = k_{ISC}/(k_{ISC} + k_D)$. The sum of both zero pressure quantum yields is unity. The intercepts of the Stern−Volmer plots therefore provide not only Φ_S but also $\Phi_T = 1 - \Phi_S$. The last column of Table 2 includes the Φ_T values derived. The data are plotted in Figure 2 to allow comparison with the results of Gandini and Hackett,[16] Horowitz,[6] and Gierczak et al.[17] Gandini and Hackett[16] determined the quantum yield of intersystem crossing directly by the triplet-sensitized emission from added 2,3-butadione. For the present purpose, the yield was estimated in 5 nm intervals from a graph for 2−4 Torr of pure acetone. Horowitz[6] measured the yield of CH_4, resulting from the reaction of CH_3 with HCl, as a function of acetone pressure and corrected for small amounts of CO produced in a side channel. Numerical values for the intercepts of Stern−Volmer plots at three wavelengths were used as given. As methyl and acetyl radicals are formed together in the same primary process, the data should be applicable. Gierczak et al.[17] measured the pressure dependence in air of quantum yields for acetone loss and CO_2 production, which were essentially equivalent, and found them to obey Stern−Volmer behavior. We have subjected the reciprocals of quantum yields reported by them to a least-squares analysis to determine the intercepts for presentation in Figure 2. Good agreement exists among all four data sets. The quantum yield for intersystem crossing is essentially nil at wavelengths below 295 nm, rises to about 0.9 between 295 and 320 nm, and remains approximately constant at longer wavelengths with an average $\Phi_T = 0.902 \pm 0.034$. Gandini and Hackett[16] found the quantum yield for intersystem crossing to approach unity at $\lambda \geq 325$ nm, but this appears to be a consequence of assumptions made in the normalization procedure used to convert relative to absolute quantum yields. Our data as well as those of Gierczak et al.[17] demonstrate that acetyl radicals are formed in this wavelength region. The combination of both data sets suggests the existence of a plateau region rather than an additional rise at $\lambda \geq 320$ nm. In the subsequent data treatment, the intersystem crossing quantum yields of Gandini and Hackett were renormalized by the above factor 0.902.

Next, we consider the effect of pressure quenching. The acetone/air mixing ratios were small enough to make quenching by acetone essentially unimportant in comparison with air despite the higher quenching efficiency of acetone. For example, Horowitz[6] reported acetone quenching constants of 0.0146 and 0.102 hPa^{-1} at 300 and 313 nm wavelength, respectively. The first is about 4.3 times, and the second about 9 times, greater than our values at similar wavelengths. Even at the highest acetone/air mixing ratio used, the contribution of acetone to the total quenching rate should be less than other uncertainties inherent in the data. Our data, therefore, are taken to describe the quenching exerted by air molecules. For comparison with the data of Gierczak et al.,[17] the Stern−Volmer slopes derived by linear least-squares treatment of all individual data sets were converted to values for k_M/k_D. The rate coefficient k_D is expected to increase with energy above the dissociation threshold; k_M may or may not depend on the excitation energy. Figure 3 shows a semilog plot of k_M/k_D versus the energy difference $\Delta E = E - E_0$, where $E = hcN_A/(10^3\lambda)$ is the excitation energy in kJ mol^{-1} and $E_0 = 353.6$ kJ mol^{-1} is the dissociation energy of acetone to yield methyl and acetyl radicals. The dissociation energy corresponds to a wavelength close to 340 nm, which lies near the origin of the absorption band. Figure 3 shows that our data and those of Gierczak et al.[17] are in excellent agreement, except our point at 330 nm. At this wavelength, as discussed earlier, the data were affected by excessive NO_2 photolysis and required extensive corrections. All the other data points fall on a straight line, indicating that k_D rises exponentially with energy. Least-squares analysis gives $\log_e(10^{20}k_M/k_D) = (5.92 \pm 0.23) - (0.073 \pm 0.005)\Delta E$ with a correlation coefficient $r = 0.975$. When the dissociation coefficient is written in the form $k_D = k_D^0 \exp(\kappa\Delta E)$, the parameters derived are $k_D^0/k_M = 2.68 \times 10^{17}$ cm^3 molecule^{-1} and $\kappa = 0.073$ mol kJ^{-1}. These results may be used to characterize the behavior of intersystem crossing as a function of excitation energy.

The dependence of intersystem crossing on excitation energy, relative to the singlet quenching rate, can be calculated from

$$k_{ISC}/k_M = (\Phi_T/\Phi_S)\, k_D/k_M = [(1 - \Phi_S)/\Phi_S](k_D^0/k_M) \times \exp(\kappa\Delta E) \quad (6)$$

We have used the individual data for Φ_S or Φ_T and the regression line shown in Figure 3 for k_M/k_D to calculate k_{ISC}/k_M. The results are plotted in Figure 4 versus the energy difference ΔE. The data carry a large statistical uncertainty arising primarily from the error propagation in forming the ratio

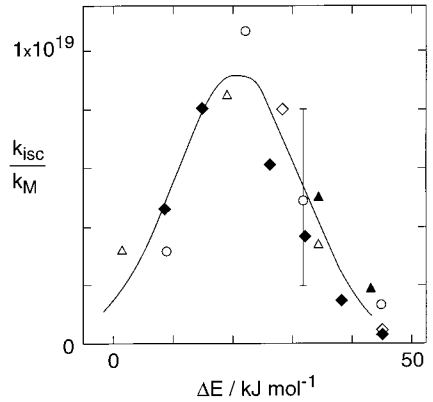

Figure 4. Relative intersystem crossing rate k_{ISC}/k_M as a function of energy above the acetone dissociation threshold. Symbols for data points are the same as in Figure 2. The curve represents a Gaussian $k_{ISC}/k_M = A \exp[-((\Delta E - \Delta E_a)/b)^2]$ with $A = (9.2 \pm 0.7) \times 10^{18}$ cm^3 molecule, $\Delta E_a = 20.7 \pm 0.9$ kJ mol^{-1}, and $b = 15.4 \pm 1.4$ kJ mol^{-1}.

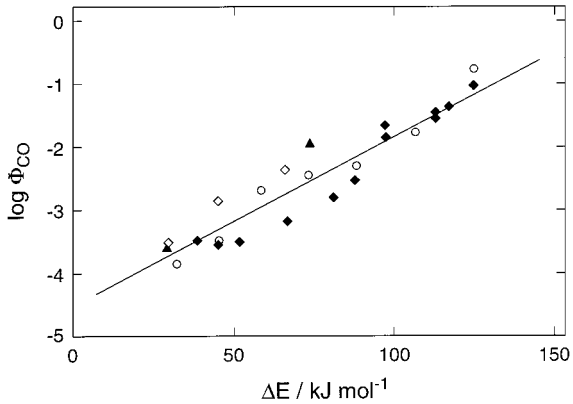

Figure 5. Natural logarithm of CO quantum yield versus energy above the acetone dissociation threshold with data from: Horowitz,[6] open diamonds; Gandini and Hackett,[16] solid diamonds; Meyrahn et al.,[18] open circles; Kirk and Porter,[27] triangles. The linear regression line is represented by $\log_e(\Phi_{CO}) = -(4.511 \pm 0.146) + (0.0266 \pm 0.0018)\Delta E$ ($r = 0.95$).

$(1 - \Phi_S)/\Phi_S$. A typical 2σ error bar is included in the figure to show the range. Despite the scatter, it is evident that the intersystem crossing rate first rises with energy toward a maximum and then declines to low values. The data may be approximated by a Gaussian, $k_{ISC}/k_M = A \exp[-((\Delta E - \Delta E_a)/b)^2]$, with $A = (9.2 \pm 0.7) \times 10^{18}$ cm^3 molecule, $\Delta E_a \approx 20.7 \pm 0.9$ kJ mol^{-1}, and $b \approx 15.4 \pm 1.4$ kJ mol^{-1}. Figure 4 includes the corresponding curve. The maximum crossing rate occurs at an excitation energy about 20 kJ mol^{-1} above the S_1 ground state at a wavelength near 320 nm. It is clear that at 313 nm, a wavelength used in many previous studies of acetone photochemistry, most of the excitation energy populates the triplet state. Toward shorter wavelengths, the rate of photodissociation from S_1 increases not only because the increase in excitation energy causes k_D/k_M to rise but also because the intersystem crossing rate declines.

Finally, it is necessary to comment on carbon monoxide as a photodecomposition product. The CO quantum yield was not determined here, but we may use the data assembled by Horowitz[6] for discussion. The origin of CO is usually assumed to be the dissociation of vibrationally hot acetyl radicals. Whereas the threshold for the process $CH_3COCH_3 \rightarrow CH_3 + CH_3CO$ coincides approximately with the origin of the absorption band, the threshold for the formation of $CO + 2CH_3$ lies at 300 nm, so at 313 nm the formation of CO from CH_3CO^* would require a contribution of thermal energy contained in the acetone molecule. This idea is supported by the observed temperature dependence of the quantum yield,[7] which increases toward unity when the temperature is raised to 125 °C. On the other hand, as emphasized by Horowitz,[6] Φ_{CO} is largely independent of pressure. This behavior would be difficult to reconcile with the pressure quenching observed for the CH_3-CO quantum yield, unless the breakup of CH_3CO^* toward CH_3 and CO is assisted by collisions. Evidence for this process has been obtained in the 313 nm photolysis of acetone and the model calculations of Nicholson.[7]

At wavelengths below about 313 nm, the CO quantum yield increases with decreasing wavelength, from $\Phi_{CO} \approx 0.025$ to $\Phi_{CO} \approx 0.45$ at 250 nm. Figure 5 shows that the CO quantum yield rises exponentially with excitation energy. The data fall on a common curve (with appreciable scatter), regardless of experimental conditions. Gandini and Hackett,[16] who studied the wavelength range 250−305 nm, used low pressures of pure acetone; Horowitz[6] worked with acetone pressures in the range 7−105 hPa (in the presence of small amounts of HCl) at wavelengths of 285, 300, and 313 nm; Meyrahn et al.[18] used mixtures of 0.1% acetone in air at near-atmospheric pressure in the wavelength range 250−310 nm. In the latter experiments, performed with NO_x-free air, the CO quantum yield at longer wavelengths was obscured by CO produced in the photolysis of formaldehyde, which arises in air from the oxidation of methyl radicals. The linear regression line shown in Figure 5 is represented by $\log_e(\Phi_{CO}) = -(4.511 \pm 0.146) + (0.0266 \pm 0.0018)\Delta E$. This equation was then used to extrapolate Φ_{CO} toward lower energies, that is, longer wavelengths. In the range $300 < \lambda < 340$ nm, the averaged CO quantum yield drops from 0.036 to 0.011.

As CO formation is observed in the presence of oxygen as well as in its absence, it appears that the addition of oxygen to the system does not stabilize vibrationally hot acetyl radicals. The CO quantum yield should also not be affected by the further addition of NO_2 to the acetone-air mixture as applied in the present experiments. Therefore, we assume that the CO quantum yield is independent of the PAN quantum yield. As a consequence, the CO quantum yield would have to be added to the PAN quantum yield at zero pressure in order to derive Φ_S as a function of wavelength. Fortunately, compared with the much larger experimental uncertainties inherent in the determination of Φ_S, the CO yields in the 300−330 nm wavelength region are still small enough to allow their neglect to a first approximation. The data in Figure 2 are affected little by not taking CO formation into account. At higher pressures, however, because of the pressure independence of CO formation, Φ_{CO} may contribute appreciably to the total decomposition of acetone. To clarify this issue, the CO quantum yield at wavelengths greater than 310 nm would have to be measured in air in the presence of a suitable scavenger so that the perturbing influence of formaldehyde formation is suppressed.

References and Notes

(1) Noyes, W. A.; Porter, G. B.; Jolly, J. E. *Chem. Rev.* **1956**, *56*, 43−94.

(2) Hoare, D. E.; Pearson, G. S. *Adv. Photochem.* **1963**, *3*, 83−156.

(3) Calvert, J. G.; Pitts, J. N., Jr. *Photochemistry*; Wiley: New York, 1966.

(4) Cundall, R. B.; Davies, A. S. *Prog. React. Kinet.* **1968**, *4*, 149−213.

(5) Lee, E. K. C.; Lewis, R. S. *Adv. Photochem.* **1980**, *12*, 1−98.

(6) Horowitz, A. *J. Phys. Chem.* **1991**, *95*, 10816−10823.

(7) Nicholson, A. J. C. *Can. J. Chem.* **1983**, *61*, 1831−1837.

(8) Greenblatt, G. D.; Ruhmann, S.; Haas, Y. *Chem. Phys. Lett*. **1984**, *112*, 200−206.
(9) Copeland, R. A.; Crosley, D. R. *Chem. Phys. Lett*. **1985**, *115*, 362−368.
(10) Haas, Y.; Ruhmann, S.; Greenblatt, G. D.; Anner, O. *J. Am. Chem. Soc*. **1985**, *107*, 5068−5074.
(11) Costela, A.; Crespo, M. T.; Figuera, J. M. *J. Photochem*. **1986**, *34*, 165−173.
(12) Heicklen, J.; Noyes, W. A. *J. Am. Chem. Soc*. **1959**, *81*, 3858−3863.
(13) Cundall, R. B.; Davies, A. S. *Proc. R. Soc. London* **1966**, *A290*, 563−582.
(14) Rebbert, R. E.; Ausloos, P. *J. Am. Chem. Soc*. **1964**, *86*, 4803−4807; **1965**, *87*, 5569−5572.
(15) Heicklen, J. *J. Am. Chem. Soc*. **1959**, *81*, 3863−3866.
(16) Gandini, A.; Hackett, P. A. *J. Am. Chem. Soc*. **1977**, *19*, 6195−6205.
(17) Gierczak, T.; Burkholder, J. B.; Bauerle, S.; Ravinshankara, A. R. *Chem. Phys*. **1998**, *231*, 229−244.
(18) Meyrahn, H.; Pauly, J.; Schneider, W.; Warneck, P. *J. Atmos. Chem.* **1986**, *4*, 277−291.
(19) Moortgat, G. K.; Seiler, W.; Warneck, P. *J. Chem. Phys*. **1983**, *78*, 1185−1190.
(20) Helas, G.; Flanz, M.; Warneck, P. *Int. J. Environ. Anal. Chem*. **1981**, *10*, 155−166.
(21) Meyrahn, H.; Helas, G.; Warneck, P. *J. Atmos. Chem*. **1987**, *5*, 405−415.
(22) Schurath, U.; Kortmann, U.; Glavas, S. In *Physico-Chemical Behaviour of Atmospheric Pollutants*, Proceedings of the 3rd European Symposium, Varese, Italy, 1984; Versino, B., Angeletti, G., Eds.; Reidel: Dordrecht, 1984; pp. 24−34.
(23) Jenkin, M. E.; Cox, R. A.; Emrich, M.; Moortgat, G. K. *J. Chem. Soc., Faraday Trans*. **1993**, *89*, 2983−2991.
(24) Wollenhaupt, M.; Crowley, J. N. *J. Phys. Chem*. **2000**, *104*, 6429−6438.
(25) Atkinson, R.; Baulch, D. L.; Cox, R. A.; Hampson, R. F., Jr.; Kerr, J. A.; Rossi, M. J.; Troe, J. *J. Phys. Chem. Ref. Data* **1997**, *26*, 521−1011, 1329−1499.
(26) Curtis, A. R.; Sweetenham, W. P. *FACSIMILE/CHECKMAT Users Manual*, Aere-R-12805; Her Majesty's Stationary Office: London, 1988.
(27) Kirk, A. D.; Porter, G. B. *J. Phys. Chem.* **1962**, *66*, 556−559.